Progress Toward Simulating Departure from Nucleate Boiling at High-Pressure Applications with Selected Wall Boiling Closures

Kim, Seung Jun
Johns, Russell Craig
Yoo, J. S.
Baglietto, Emilio

To be published in: Nuclear Science and Engineering

DOI to publisher's version: 10.1080/00295639.2020.1743579

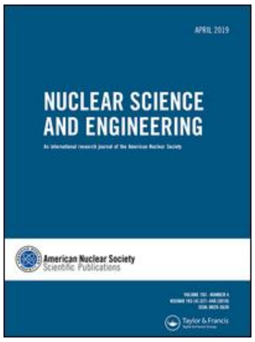

Taylor & Francis
Taylor & Francis Group

Nuclear Science and Engineering

ISSN: 0029-5639 (Print) 1943-748X (Online) Journal homepage: https://www.tandfonline.com/loi/unse20

Progress Toward Simulating Departure from Nucleate Boiling at High-Pressure Applications with Selected Wall Boiling Closures

Seung Jun Kim, Russell C. Johns, Junsoo Yoo & Emilio Baglietto

To cite this article: Seung Jun Kim, Russell C. Johns, Junsoo Yoo & Emilio Baglietto (2020): Progress Toward Simulating Departure from Nucleate Boiling at High-Pressure Applications with Selected Wall Boiling Closures, Nuclear Science and Engineering, DOI: 10.1080/00295639.2020.1743579

To link to this article: https://doi.org/10.1080/00295639.2020.1743579

NUCLEAR SCIENCE AND ENGINEERING

DOI: https://doi.org/10.1080/00295639.2020.1743579

Progress Toward Simulating Departure from Nucleate Boiling at High-Pressure Applications with Selected Wall Boiling Closures

Seung Jun Kim,[a]* Russell C. Johns,[a] Junsoo Yoo,[b] and Emilio Baglietto[c]

[a] *Los Alamos National Laboratory, P.O. Box 1663, Los Alamos, New Mexico 87545*
[b] *Idaho National Laboratory, 2525 Freemont Avenue, Idaho Falls, Idaho*
[c] *Massachusetts Institute of Technology, Cambridge, Massachusetts 02139*

Received December 18, 2019
Accepted for Publication March 10, 2020

Abstract — *Recently, a Eulerian-based two-fluid computational fluid dynamics (CFD) framework with a wall heat flux partitioning approach has been intensively investigated for departure from nucleate boiling (DNB) simulation under the U.S. Department of Energy–funded Consortium for Advanced Simulation of Light Water Reactors (CASL) program. Understanding of the DNB characteristics over a range of pressurized water reactor–like operating conditions and accurate prediction of boiling crisis in the nuclear power system have been grand challenges because of the large impact of DNB on reactor safety and operational economics. The ultimate goal of this task in the CASL program is to introduce a robust multiphase CFD–based DNB modeling framework that is capable of characterizing an entire boiling history in which the wall boiling mode experiences the following through multiple stages of heat transfer mode: (1) single-phase convective heat transfer, (2) nucleate boiling heat transfer, and (3) identification of the departure of nucleate boiling. To validate the CASL boiling model, we have benchmarked simulated DNB over three different flow channel configurations (pipe flow, 5 × 5 fuel bundle with mixing vane tests, and 5 × 5 fuel bundle without mixing vane tests) against experimental measurements, and the validation result with open literature is reported. The DNB detection criteria in the simulation are checked by monitoring the peak wall temperature, wall dryout factor, and net energy balance. In addition to the DNB performance test, some preliminary sensitivity results on closure model selection are reported to address the prediction capability of local void profile against measurements. The boiling simulation tested in this study exhibits a maximum deviation of 24% from the measured DNB value in a high-pressure (i.e., 138 bars) subcooled pipe flow test. The ranges of operating conditions are as follows: 1650 to 2650 kg/m^2·s for mass flux and 8.5 to 96 K for subcooled inlet temperature. The deviation is even reduced to 7% when the subcooled temperature is less than 40 K. Besides accuracy, base practice guidelines for DNB detection criteria are tested by monitoring three simulation variables: (1) maximum wall temperature, (2) wall dryout factor (i.e., K-value), and (3) energy balance. Numerical robustness of DNB simulation is largely achieved in most of the validation test except for a few high subcooled test cases.*

Keywords — *Departure from nucleate boiling simulation, multiphase CFD, wall boiling closures.*

Note — *Some figures may be in color only in the electronic version.*

I. INTRODUCTION

Subcooled flow boiling can provide an effective heat transfer mode in a heat flux–controlled system like a pressurized water reactor (PWR). This enhanced heat transfer mode, however, is limited by critical heat flux (CHF) or departure from nucleate boiling (DNB). Beyond

*E-mail: skim@lanl.gov

this critical point, the system encounters a radial reduction of the heat transfer coefficient (HTC) due to the transition from nucleation boiling to the film boiling condition and experiences a temperature excursion at the heating surface that hampers the safety and integrity of the heating surface of the fuel rods. In PWRs, CHF or DNB prediction is a critical design parameter and an important operational issue as it is related to reactor safety and economics.[1] One of the key deliverables in this work is to demonstrate the DNB modeling capability for subcooled flow boiling application under PWR operating conditions. Over the past 4 years, the Consortium for Advanced Simulation of Light Water Reactors (CASL) Thermal Hydraulic Method (THM) team has been extensively demonstrating the DNB modeling capability for subcooled flow boiling application for a high-pressure operating condition. The CASL boiling model is implemented with a commercial computational fluid dynamics (CFD) package, STAR-CCM+ v12.06.010, to assess the predictive capability with the various flow configurations. Previous DNB validation campaign efforts are summarized as follows:

1. In fiscal year 2016 (FY16), the CASL baseline model was developed and tested for pipe flow DNB. A virtual boiling test methodology was proposed to evaluate the DNB predictive performance. The baseline boiling closures were selected and implemented into a simple pipe flow DNB test at the high-pressure condition (e.g., 138 bars). The predicated DNB was directly compared to corresponding measurements showing underpredictive behavior up to 33% deviation.[2]

2. In FY17, we performed a DNB test of a 5 × 5 fuel bundle flow configuration with and without mixing vane spacer grids. Basically, the same baseline model was tested in more complex configurations showing similar underpredictive behavior (i.e., ~50%) (Ref. 3).

3. In FY18, we scrutinized the baseline boiling model and identified what would be the potential cause of underprediction.[3] A series of closure sensitivity studies on void and DNB was conducted, and the CASL modified boiling model is proposed for high-pressure DNB application.[4]

4. In FY19, we reevaluated the DNB prediction performance with the modified CASL model for a pipe flow subcooled boiling test at the high pressure.[5]

As a practical method to analyze and predict the two-phase boiling phenomena, most commercial CFD codes have employed the two-fluid Eulerian-Eulerian model framework. Under this framework, the role of closure models (or closure relations), which capture relevant interphase physics, is critical, and hence, a great deal of effort has been paid over the last decades to develop the closure models in either empirical or mechanistic fashion. In parallel, considerable effort has been devoted toward finding the optimal combination of "existing" closure models, aiming to predict the widest possible range of subcooled flow boiling conditions. However, because of the inherent complexity of subcooled flow boiling phenomena, those efforts have yet to yield satisfactory results, and similar endeavors are still underway.[6]

This paper aims to provide a comprehensive summary of the boiling model study for high-pressure DNB application over the CASL project and to identify the current predictive capability using CASL boiling closure; potential research is for future work. This paper is divided into four main parts. Section II summarizes the numerical description of the CASL boiling model with selected interfacial transport closure. A detailed discussion on the selected wall boiling model and desirable DNB detection criterion are reported in Sec. III. A sensitivity study of the closure model, which is performed to support the present closure model setup for DNB prediction, is summarized in Sec. IV. Preliminary results of DNB performance and simulated boiling characteristics are discussed in Sec. V. Finally, conclusions and suggested future work are presented in Sec. VI.

II. NUMERICAL DESCRIPTION OF CASL BOILING MODEL

In general, the CASL boiling model tracks the local void fraction near the heated surface to identify the inception of the DNB that transitions from the nucleate boiling state to the film boiling stage. When it comes to the local void fraction in the model, interfacial liquid-vapor mass, momentum, and energy equations are solved to close the system of conservation equations. In the DNB simulations all the voids are created at the heated surface by a calculation of evaporation mass flux that is converted from the evaporation heat flux using the latent heat energy equation. Therefore, an accurate evaporation heat flux calculation is a significantly important variable to quantify the void information near the wall. In particular, the current boiling model is based on the bubbly layer theory proposed by Weisman and Pei.[7] The DNB criterion is based solely on the void fraction near the wall in the computation cells. In order to accurately predict the boiling crisis in the CFD model, the void transfer mechanism should be carefully examined in the wall boiling closure as well as associated interfacial momentum closures.

However, it should also be noted that both interfacial momentum transfer closures and wall boiling closures are highly dependent on the interfacial length scale and the bubble size distribution at the operating conditions. In addition, the applicability of the selected closures at high-pressure operating conditions should be also taken into consideration for the DNB boiling test. An overall numerical approach for the DNB boiling simulation is briefly summarized below. The closure models are selected by considering the following three factors: (1) physical correctness, (2) predictive capability, and (3) numerical robustness for DNB application. The detailed multiphase interfacial closures and boiling closure correlations are listed in Table I.

II.A. Eulerian-Based Two-Fluid Conservation Equations

In the two-fluid model, mass, momentum, and energy equations are modeled for each phase in conjunction with an interfacial transport term. A brief description on the transport equation applied is summarized below with an interpretation related to the interfacial transport concept.

The conservation of mass for phase k is

$$\frac{\partial}{\partial t}(\alpha_k \rho_k) + \nabla \cdot (\alpha_k \rho_k u_k) = \sum_{i=1}^{N} (\dot{m}_{ki} - \dot{m}_{ik}) \tag{1}$$

and

$$\sum_k \alpha_k = 1, \tag{2}$$

where

α_k = volume fraction of phase k

ρ_k = phase density

u_k = phase velocity

$\dot{m}_{ki}$, $\dot{m}_{ik}$ = mass transfer rates to and from the phase, respectively

N = total number of phases.

Note that the mass transfer rate in the mass conservation equation is calculated based on the void generation (i.e., liquid phase to vapor phase) by the evaporation term

TABLE I

Gen1-FY19 CASL Boiling Closure Selection for High-Pressure DNB Application

Interfacial Transfer and Boiling Closure	Selected Model and Correlation
Interfacial Momentum/Energy Transfer	
Lift force Drag force Turbulence dispersion force Wall lubrication force	Sugrue-Podowski lift Tomiyama et al. model with contamination Turbulent dispersion Pr = 1.0 Lubchenko et al. model
Interphase Mass/Energy Transfer	
Liquid phase condensate Vapor phase condensate Interfacial area density Interaction length scale	Kim-Park condensation model Nu = 26 Symmetric particle assumption S-gamma with Sauter mean diameter (limiter: 1e-6 m; coalescense coefficient: 0.2)
Wall Boiling Model	
Convective heat flux Evaporation heat flux Quenching heat flux Wall boiling relaxation Wall dryout area fraction	Single-phase turbulent convection model Bubble departure diameter: Kocamustafaogullari Bubble departure frequency: Cole Nucleation site number density: Modified Li et al. model Quenching HTC: Del Valle Kenning model Bubble-induced fraction: Kurul-Podowski Wall boiling underrelaxation factor: 0.5 Wall dryout breakpoint: 0.9 Bubbly layer relaxation faction: 1.0 Bubbly layer option: fixed Y+: 200

in wall boiling closure and liquid generation (i.e., vapor phase to liquid phase) by the condensate model at the bulk fluid region.

The conservation of momentum for phase k is

$$\frac{\partial}{\partial t}(\alpha_k\rho_k u_k) + \nabla\cdot(\alpha_k\rho_k u_k u_k) - \nabla\cdot\left(\alpha_k\left(\tau_k + \tau_k^t\right)\right) = -\alpha_k\nabla P + \alpha_k\rho_k g + M \quad (3)$$

and

$$M = F_D + F_{TD} + F_L + F_{VM} + F_{WL} + \sum_{i=1}^{N}(\dot{m}_{ki}u_k - \dot{m}_{ik}u_i), \quad (4)$$

where

τ_k, τ_k^t = laminar and turbulence shear stresses, respectively

P = pressure

M = sum of the interfacial momentum transfer that includes drag, lift, wall lubrication, turbulence disperse force, and virtual mass force.

The conservation of energy for phase k is

$$\frac{\partial}{\partial t}(\alpha_k\rho_k h_k) + \nabla\cdot(\alpha_k\rho_k u_k h_k) - \nabla\cdot\left(\alpha_k\left(\lambda_k\nabla T_k + \frac{\mu_t}{\sigma_h}\nabla h_k\right)\right) = Q \quad (5)$$

and

$$Q = \alpha_k\frac{DP_k}{Dt} + \alpha_k\left(\tau_k + \tau_k^t\right):\nabla u_k + \sum_{i\neq k} Q_{ki} + \sum_{(ik)} Q_k + \sum_{i\neq k}(m_{ki}h_k - m_{ik}h_k), \quad (6)$$

where

h_k = phase enthalpy

λ_k = thermal conductivity in phase k

T = temperature

μ_t = turbulent viscosity

σ_h = turbulent Prandtl number

Q = interfacial heat transfer and other heat source.

Again, note that the void creation term (i.e.,m_{ki}) by evaporation and the liquid generation term (i.e.,m_{ik}) by the condensate models are used in Eq. (6) to quantify interfacial energy transfer Q. Thus, a selection of appropriate wall boiling closures (void generation) and condensate (liquid generation) models are very important since they are tightly coupled with interfacial mass and energy conservation.

II.B. Thermodynamic Properties, Meshing Strategy, and Boundary Conditions

In the current simulation, thermodynamic properties for the liquid and vapor phases are defined by the "IAPWS Industrial Formulation 1997 for the Thermodynamic Properties of Water and Steam"[8] (IAPWS-IF97) correlation at the given system pressure and temperature. The correlation provides a fundamental polynomial equation for the specific Gibbs free energy, and then, the density and other thermodynamic properties are calculated for both liquid and vapor based on the correlation.[8] Thus, the density and all thermodynamic properties (e.g., viscosity, heat capacity, and latent heat) for the liquid and vapor phases are changed along with the flow condition. Temperature- and pressure-dependent thermodynamic properties are selected as it is believed that the dynamic model captures the realistic thermodynamic properties in a two-phase environment. It is also worth noting that all simulation cases in this study fall within the validity window; thus, no numerical issue with the IAPWS-IF97 feature is observed in the current test.

The standard k-ε turbulence model with high Y+ wall treatment is selected to solve turbulent flow in both phases. Bubble-induced turbulence is not considered in this study as Magolan and Baglietto in their work have investigated a balance between production and dissipation of bubble-induced turbulence at a high-Reynolds-number condition and concluded that shear-induced turbulence is the dominant component.[9] In general, turbulence effects on various fluid applications should be a checking point for high-fidelity calculations. In this bubbly flow condition with void fractions below 30%, however, the shear-induced component is dominant, and the adoption of the standard k-ε approach provides reasonable predictions on DNB performance. However, there might be some effect on the void profile in the radial direction associated with different turbulence models since the turbulence dispersion force might be slightly changed between turbulence models.

The CFD model domain represents the exact geometry and test condition of the reference experiments reported by Weatherhead.[10] The experiments were performed at varying operating conditions that affected the flow boiling characteristics and DNB performance. Weatherhead explicitly described tube channel geometry, mass flux, system pressure, inlet temperature, and calculated exit quality based on the energy balance. In regard to meshing strategy, the CFD domain is modeled in only one-fourth of the tube geometry by implementing the symmetry boundary condition, which enables the model to lower the computational cost without a loss of physics. A hexahedral-dominant mesh (Fig. 1) is used, and the total number of cells is approximately 0.4 million. The base size of 0.2 mm was chosen in the bulk fluid domain with two layers of prism mesh next to the heated wall. The near-wall prism mesh has a total thickness of 0.5 mm, resulting in the wall y^+ value lying within the logarithmic region of the boundary layer for all the test cases (typically $y^+ \sim 100$). A mesh sensitivity study on the boundary layer and bulk flow region was performed to find an optimal mesh provding a robust numerical simulation with reasonable predictive performance on DNB. It was observed that a finer mesh ($y^+ \sim 1$) near the wall results in a notable instability in the two-phase flow solver and poor interfacial variable convergence. Refinement of the mesh in the bulk flow region did not affect the DNB prediction. The length of the heated section is 47.5 cm with a 10-cm unheated zone before and after the heated section. The uniform heat flux is applied on the heated wall surface along with the flow direction. The boundary condition for the inlet is defined as a fully developed pipe flow profile with a fixed temperature, and the outlet is set to a pressure-out condition.[11]

II.C. Interfacial Radial Momentum Transfer and Interfacial Area Transfer Model

Equation (4) represents the sum of five key momentum sources ($F_D + F_{TD} + F_L + F_{VM} + F_{WL}$). Those interfacial momentum transfer models can be divided into two groups: (1) drag force and (2) nondrag force. Drag force usually governs interfacial momentum transfer along with flow direction that is not directly related to lateral void distribution. Nondrag forces include lift force F_L and wall lubrication force F_{WL}. The combination of nondrag forces determines the lateral void distribution encompassing the near-wall boiling region and bulk fluid region. Since void prediction is a most critical variable for the DNB triggering algorithm, nondrag force closure should be examined and validated with high-resolution void distribution experimental data. However, most DNB tests report only system extrema such as CHF, exit outlet temperature, and some pressure drop. Thus, high-resolution void data are rarely obtained from any open literature. Unfortunately, this is a most challenging component in a successful DNB model validation test.

The drag force model has two components: an average part and a fluctuating part. The average drag force is given by

$$F_D = \frac{3\alpha_g \rho_l}{4d_B} C_D \alpha_g^4 \left|u_l - u_g\right| (u_l - u_g) \quad , \tag{7}$$

where d_B is the bubble diameter and $C_D$is the drag coefficient, estimated by Tomiyama et al.[12] for a mildly contaminated two-fluid system. The fluctuation part of the drag force is usually calculated as the turbulent dispersion force, which plays an important role in taking the vapor bubbles from the near-wall region to the bulk liquid:

$$F_{TD} = -2\frac{\nu_l^t}{\alpha_g \alpha_l \sigma_a} \nabla \alpha_g \quad , \tag{8}$$

where ν_l^t is the turbulent kinematic viscosity of the liquid phase and σ_a is the turbulent Prandtl number (default value of 1 is used in this study).

Regarding nondrag forces, lift and wall lubrication force models are newly implemented in the FY19 boiling model. The current study implements the Sugrue lift model[13] incorporating a wobbly bubble effect and the Lubchenko et al. model[14] accounting for a wall lubrication effect based on the postulated liftoff diameter concept

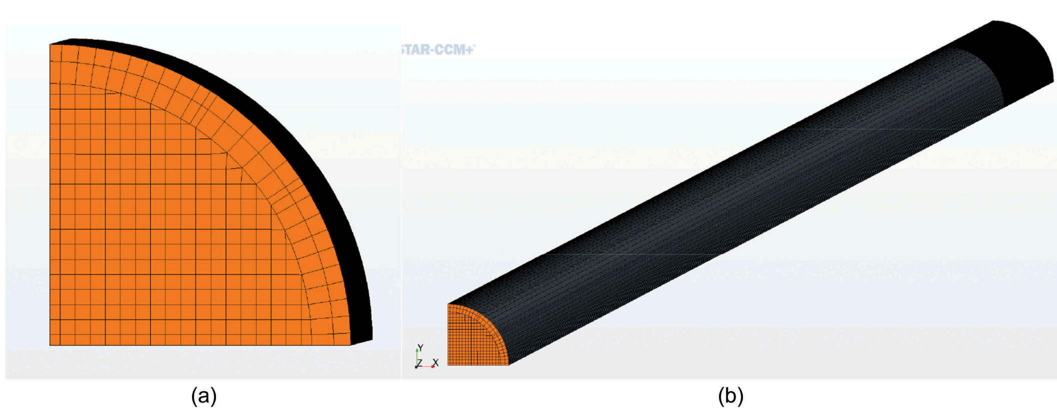

Fig. 1. (a) Mesh in the outlet plane and (b) mesh on the heated wall with iso-view.

developed by Massachusetts Institute of Technology. Those newly adopted boiling closures can help an improved lateral void estimation at the near wall, which will prevent the premature DNB triggering mechanism observed in the previous validation campaign:

$$F_L = C_{L,Sugrue} \alpha_g \rho_l \left[\left(u_l - u_g \right) \times \left(\nabla \times u_l \right) \right] \tag{9}$$

and

$$F_{WL} = -C_{WL,Lubchenko}(y_w) \alpha_g \rho_l \frac{\left| u_l - u_g \right|^2}{d_B} \quad . \tag{10}$$

As described earlier in this section, it is also critical to correctly model a set of multiphase interfacial area transport closures as those closures play a significant role in the mass, energy, and momentum equations [see Eqs. (1), (3), (5), and (6)]. Phase change between liquid and vapor can be modeled as vapor generation by evaporation near or at the wall and liquid generation by condensation in the subcooled bulk fluid region. With this in mind, the bubble size distribution is one of many unknowns in the subcooled flow boiling regime due to lack of high-resolution experimental measurement at a certain pressure condition. In the current study, the Sauter mean bubble diameter distribution is calculated with a two-equation S-gamma model. Unlike Kurul-Podowski's interfacial area transfer model correlating the bubble diameter with only the function of the subcooled temperature at a fixed pressure condition, the S-gamma model captures the bubble diameter distribution in the subcooled boiling flows by resolving the mechanistic moment transfer equation.[15] The S-gamma model is a model similar to the interfacial area transfer equations including a set of chaotic bubble dynamics such as bubble breakup and coalescence, but their source items are different. The S-gamma model represents the bubble size distribution using the method of moment approach. Thus, the bubble size distribution is assumed to have a predefined shape, and this shape is retained during the bubble profile calculation. A detailed description of the S-gamma model can be found in Lo and Rao's paper.[16]

III. WALL BOILING CLOSURES

In parallel to closures related to void distribution, wall boiling closures are effectively contributing to the void profile calculation near the wall, which is the sole criterion of DNB detection in the current approach shown in Fig. 2. In general, the wall heat flux can be viewed as three parts according to the wall heat partitioning model: (1) single-phase convective heat flux, (2) evaporative heat flux, and (3) quenching heat flux. The wall dryout

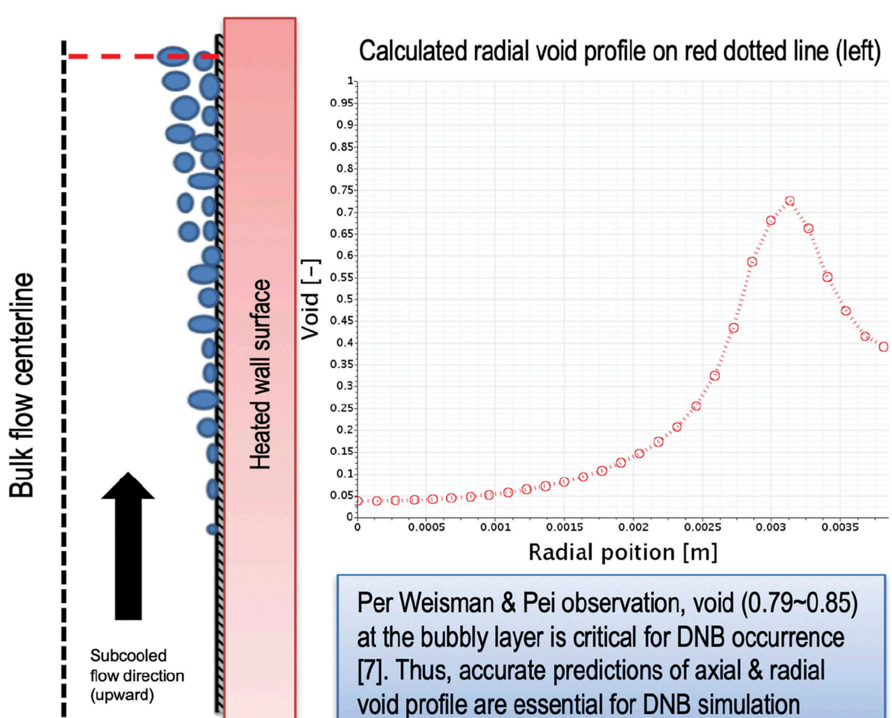

Fig. 2. DNB detection criterion based on a void profile near the wall.

factor K_{dry} is utilized to smoothly transition the nucleate flow boiling mode to film boiling by the vapor-only heat transfer mode shown as

$$q''_w\left(q''_{Conv.liquid} + q''_{Evaporation} + q''_{Quenching}\right)(1 - K_{dry}) + q''_{Conv.vapor}K_{dry} \quad , \tag{11}$$

where K_{dry} is a mathematical function composed of local void fractions at a certain distance from the wall (see Ref. 2 for detailed information). Equation (11) numerically illustrates how the wall boiling model operates from subcooled nucleate boiling (i.e., normal mode) to DNB (i.e., DNB mode). There are two conditions incorporated in the wall boiling model. The first term in Eq. (11) reflects a normal nucleate boiling regime in which the heat flux is still well below DNB, while the second term describes a DNB condition when bubble generation starts sufficiently covering the heated surface and finally turns into a film boiling condition:

$$q''_{Conv.liquid} = \frac{\rho_l C_{p,l} u_l^*}{T_l''+}(T_w - T_l) \quad , \tag{12}$$

$$q''_{Quenching} = 2K_{quenching} f\sqrt{\frac{\rho_l C_{p,l} k_l t_w}{\pi}}(T_w - T_{l,quench}) \quad , \tag{13}$$

and

$$q''_{Conv.vapor} = \frac{\rho_v C_{p,v} u_v^*}{T_v^+}(T_w - T_v) \quad , \tag{14}$$

where

$u_l^*,\ u_v^*$ = velocity of liquid and vapor near the heated wall surface, respectively

$T_l^+,\ T_v^+$ = nondimensional parameters for liquid and vapor, respectively; those near-wall velocities and dimensionless temperature parameters are all calculated through wall functions

$C_{p,l},\ C_{p,v}$ = liquid and vapor specific heat, respectively

$K_{quenching}$ = bubble influence area coefficient.

Among the three heat flux partition terms in the wall modeling model, the evaporation heat flux term dominates mostly the wall dryout factor as it determines the void creation. As the current DNB triggering mechanism is purely based on a local void near wall, the void generation term calculated by the evaporation heat flux must be a more practical calibration factor from the DNB prediction performance standpoint. Thus, the evaporation heat flux term should be carefully calibrated for the desired applications (e.g., high-pressure flow boiling DNB):

$$q''_{Evaporation} = N_a f_d\left(\frac{\pi D_d^3}{6}\right)\rho_g h_{fg} \quad , \tag{15}$$

where

N_a = active nucleation site density (NSD)

D_d = bubble departure diameter (BDD)

f_d = bubble departure frequency (BDF).

Equation (15) implies the amount of equilibrium evaporation heat flux multiplied by the mass flux of bubble generation multiplied by the latent heat and vapor density at the given system pressure (i.e., NSD × BDD × BDF). Thus, one should have a wise selection of three wall boiling closures to quantitatively calculate the evaporative heat flux. More detailed discussion on those closure selections are discussed below.

III.A. Active Nucleation Site Density

In the FY19 model, active NSD is estimated by the modified Li et al. model.[17] Li et al.'s NSD model strives to account for the system pressure, surface characteristics, and wall superheat when NSD is correlated based on empirical data with a wide range of operating pressure conditions illustrated in Fig. 3. In addition to Li et al.'s model, we implement a limiter factor in the Li et al. model to account for the possible maximum NSD value from analytic calculations based on bubble size. It is noted that this limiter factor helps to keep the numerical robustness of the current boiling simulations by preventing the NSD value from increasing excessively.

III.B. Bubble Departure Diameter

The BDD model determines the diameter of departing bubbles at the heated wall when it leaves the nucleation site. Along with NSD, BDD is one of the most challenging wall boiling closure models. While there exist numerous analytic correlations and semiempirical models, a viable BDD at conditions of high pressure and flow boiling is still yet to be introduced. In this study, BDD is estimated by the Kocamustafaogullari model[18]:

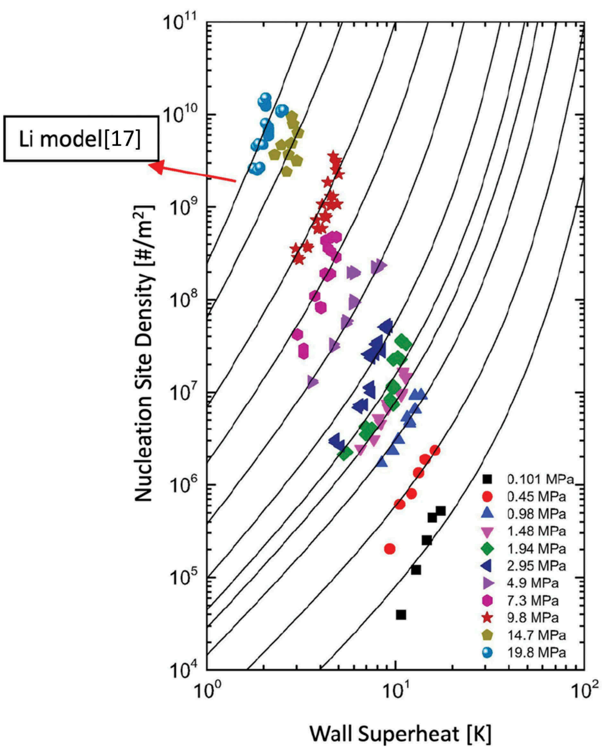

Fig. 3. Nucleation site density by Li et al. and experimental data at different pressures.[17]

$$d_d = 2.64 \times 10^{-5}\theta\sqrt{\left(\frac{\sigma}{g\Delta\rho}\right)\left(\frac{\Delta\rho}{\rho_g}\right)^{0.9}} . \tag{17}$$

According to the Kocamustafaogullari model and comparison against experimental data, BDD varies widely with different pressures. For example, at 1 bar, BDD by the model is calculated to be 2 mm, but the value reduces to 0.006 mm at high pressure (e.g., 138 bars) as shown in Fig. 4. The validity of the Kocamustafaogullari model is not evaluated in this study due to lack of available experimental measurements; however, it should be noted that a change in BDD inevitably leads to more calibration in other closures (e.g., BDF and active NSD).

III.C. Bubble Departure Frequency

The BDF model follows Cole's approach.[19] Cole assumes that a typical bubble rise velocity is determined by BDD using a force balance at the bubble departing surface:

$$f = \sqrt{\frac{4g\left(\rho_l - \rho_g\right)}{3D_d\rho_l}} . \tag{18}$$

This model is originally developed for nucleate pool boiling at the horizontal heat transfer surface. Thus, the validity of the Cole model on the vertical boiling heat transfer surface requires further investigation. Although there are several other BDF models available in the literature, this study selects the Cole model because of its simplicity in implementation and numerical robustness. In the Cole model, the

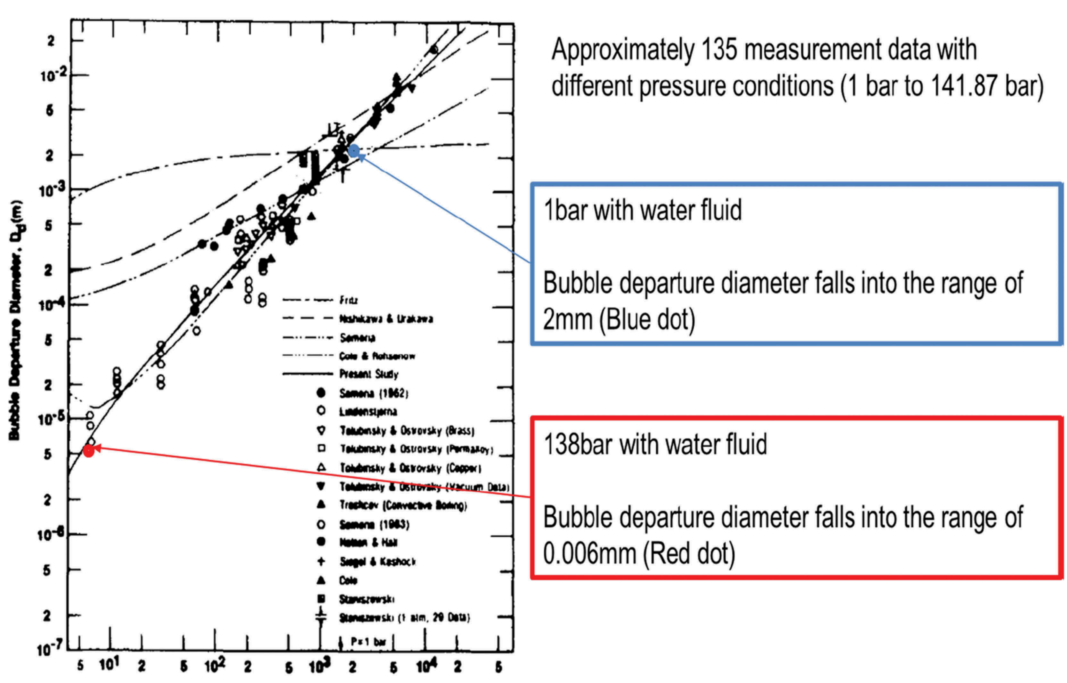

Fig. 4. Bubble departure diameter with pressure (Kocamustafaogullari model).[18]

waiting time between the bubble departure and the activation of the next bubble is assumed to be 80% of the total bubble departure time in the pool boiling scenario. Therefore, a compounding effect between the departure diameter and frequency should be accounted for when the wall boiling closures are selected for the desired DNB model for high-pressure subcooled flow boiling application.

IV. WALL BOILING CLOSURE SENSITIVITY ON VOID PROFILE PREDICTION

As discussed in Sec. III, the void distribution is one of the most important factors affecting the DNB prediction. Accordingly, the present study has performed a boiling closure sensitivity study to investigate the impact of model selection on prediction of the void profile at PWR-like high-pressure subcooled flow boiling conditions. Particularly, this study has adopted the experimental data from two papers from Bartolomei and Chanturiya[20] and Bartolomei et al.[21] The so-called Bartolomei experiment was performed in subcooled boiling conditions of water flowing upward through a vertical heated pipe over a range of operating pressure (up to 15 MPa), mass flux (up to 2000 kg/m^2°s), and heat flux (up to 2.2 MW/m^2) conditions.

In the experiment, the cross-sectional area-averaged void fractions were measured at different axial locations, while the heated wall and subcooled liquid temperatures were also available for one experimental condition (this is used in this paper as base case T1 as shown in Table II). The void fractions were measured by detecting the gamma-ray penetration through the flow boiling channel from a Tu-170 source. These measurements were performed for several different sizes of pipe, but the experimental data from the pipe (inner) diameters of 15.4 and 12 mm were particularly used for the present discussion. The heated length of the vertical pipe was about 2 and 1.5 m for the 15.4- and 12-mm-diameter pipes, respectively. The details of the experimental conditions used in this study are summarized below.

IV.A. Assessment of Wall Boiling Models

Nucleation site density calculates the number of departing bubbles on the heated surface over a unit area. In the previous validation tests, we tested two methods: (1) the Lemmert-Chawla model[22] and (2) the Hibiki-Ishii model.[23] Both models were basically correlated based on various experimental measurements. Usually, the original Lemmert-Chawla model predicts a relatively smaller site density compared to the Hibiki-Ishii model at a given pressure condition.

The first model assessment was performed with regard to the evaporation term in the wall boiling model, specifically the BDD and the active NSD models. The two widely used pairs of the BDD and the NSD models are (1) Tolubinsky-Kostanchuk + Lemmert-Chawla and (2) Kocamustafaogullari + Hibiki-Ishii. For the present subcooled flow boiling simulations, the Li et al. NSD model is adopted as a replacement for the Hibiki-Ishii NSD model. The Hibiki-Ishii model is known to predict extremely high values of active NSD as the heat flux or wall temperature increases at high-pressure conditions. Since the simple Rensselaer Polytechnic Institute (RPI) model does not account for the inevitable interaction between active bubbles and sites occurring in a realistic scenario, the effective number of sites cannot be limited. As a result, the Hibiki-Ishii model often causes unphysically high nucleation site densities, which leads to severe code stability problems. Li et al.'s NSD model exhibits better agreement with the effective number of active sites measured at high-pressure conditions. Indeed, by replacing the exponential form presented in the Hibiki-Ishii model with the power law form, Li et al.'s model predicts a milder increase in NSD with heat flux under high-pressure conditions.

It is therefore expected that the Li et al. NSD model can alleviate the code stability and provide a more realistic representation of NSD. Figure 5 compares the wall temperature (blue color) and cross-sectional averaged void fraction (red color) along the axial channel direction, for the different BDD

TABLE II

Experimental Cases of Bartolomei Used for Wall Boiling Closure Sensitivity Study

Test Number	Tube Inner Diameter (m)	Pressure (MPa)	Mass Flux (kg/m^2·s)	Heat Flux (MW/m^2)	T_{in} (K)	$\Delta T_{sub,in}$
T1 (base case)	0.0154	4.50	900	0.57	472.4	58.2
T34	0.0120	14.79	1878	0.42	603	11.2
T37	0.0120	14.70	2014	1.72	545	68.7

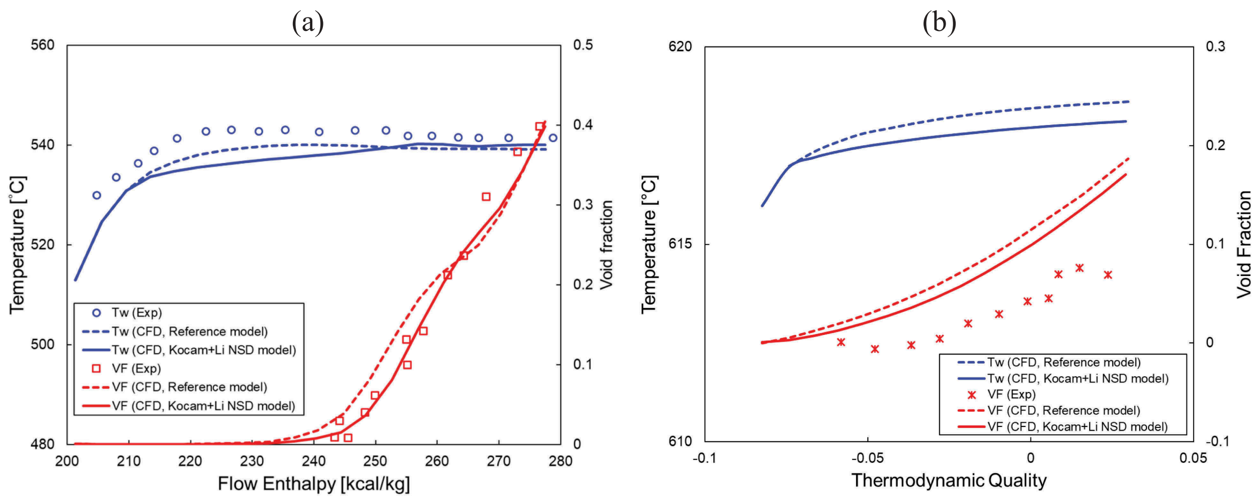

Fig. 5. Effect of BDD and nucleation site number density models on the wall temperature and void fraction prediction along the axial channel direction: (a) T1 and (b) T34.

and NSD model pairs, i.e., (i) Tolubinsky-Kostanchuk + Lemmert-Chawla (reference model, dotted line) and (ii) Kocamustafaogullari + Li et al. (solid line). The experimental data are presented as symbols when available. The *x*-axes are displayed as the cross-sectional averaged flow enthalpy or thermodynamic quality, instead of the axial channel position, for comparison with the experimental data. In Fig. 5, two cases of the Bartolomei experiment performed at different test conditions and tube diameters, T1 (relatively low pressure) and T34 (high pressure), are used for comparison; the experimental conditions are detailed in Table II. Compared to the case of model (i) [reference model in Fig. 5], model (ii) tends to underestimate the wall temperature and overestimate the void fraction for both cases, but the difference of the simulation results between models (i) and (ii) is insignificant. Also, both models (i) and (ii) significantly overpredict the void fraction measured at conditions of higher pressure and higher heat flux (see Fig. 5b). It is noted that despite the insignificant difference in the prediction of the void fraction between models (i) and (ii), there was significant difference in the prediction of fundamental bubble parameters, such as BDD, BDF, and the active NSD, between the two models. For the present high-pressure boiling simulations, it is argued that model (ii) be preferred since model (i) does not account for the pressure effect.

IV.B. Assessment of Interaction Length Scale Models

In multiphase CFD (M-CFD) simulations, the interaction length scale refers to a characteristic length scale used to control the interfacial area density as well as other required modeling quantities such as the bubble Reynolds number Re_b. In bubbly flow, the interaction length scale can be used to simply represent the mean bubble size that interacts with the continuous phase. In the FY17 CASL boiling model, the interaction length scale is determined by the Kurul-Podowski model, in which the interaction length scale is correlated with the subcooling liquid temperature ΔT_{sub} as follows:

$$l_{cd} = \frac{D_{min}\left(\Delta T_{D,max} - \Delta T_{sub}\right) + D_{max}\left(\Delta T_{sub} - \Delta T_{D,min}\right)}{\Delta T_{D,max} - \Delta T_{D,min}} , \tag{19}$$

where

D_{min}, D_{max} = minimum and maximum bubble diameters, respectively (the default values are D_{min} = 0.15 mm and D_{max} = 2 mm)

$\Delta T_{D,max}$, $\Delta T_{D,min}$ = liquid subcooling degree corresponding to D_{max} and D_{min}, respectively (the default values are $\Delta T_{D,max}$ = −5 K and $\Delta T_{D,min}$ = 13.5 K).

Equation (19) indicates that the Kurul-Podowski model computes the interaction length scale l_{cd} based only on the subcooling temperature, meaning that the mean bubble size within the bulk liquid is determined regardless of the characteristics of bubbles caused by wall boiling. In other words, the interaction length scale model is decoupled from the wall boiling models. To investigate this issue further, the S-gamma model, which accounts for the bubble size distribution in the bulk liquid, is additionally employed to the current study. Figure 6 shows that the predicted values of the void

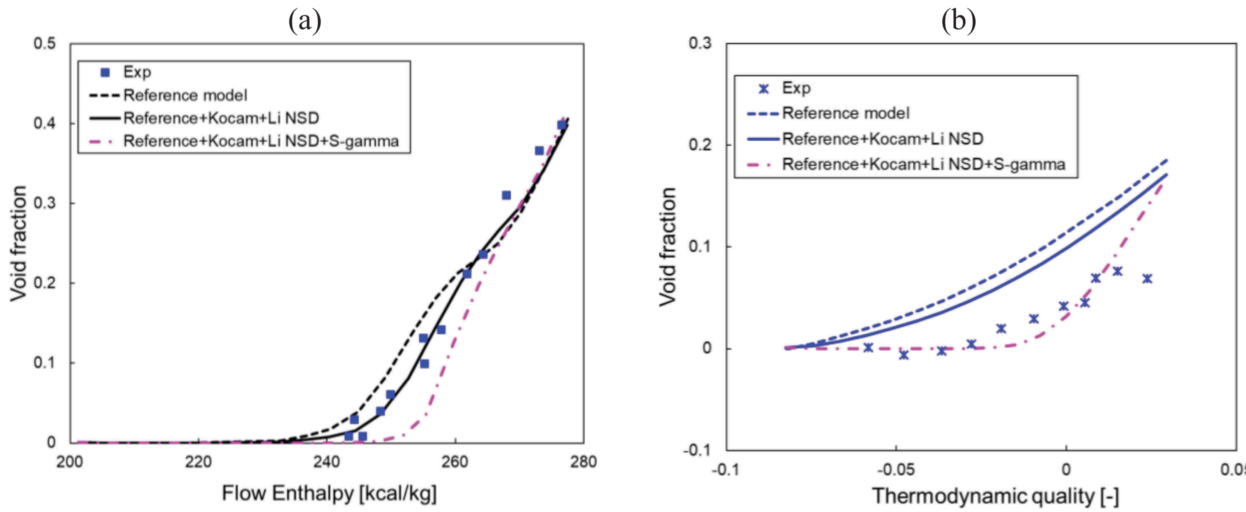

Fig. 6. Effect of applying S-gamma model on the prediction of averaged void fraction: (a) T1 and (b) T34.

fraction become significantly lower by using the S-gamma model. Another observable difference is that the point of net vapor generation, where the net void fraction starts to increase, is significantly retarded by the S-gamma model.

IV.C. Assessment of Interfacial Heat Transfer Model

As for the interfacial heat transfer, especially condensation heat transfer in the bulk liquid, the Ranz-Marshall correlation[24] has been most widely used in previous CFD boiling studies. Despite its popularity, however, it should be noted that the Ranz-Marshall correlation was not developed directly for condensing steam bubbles but was developed for evaporating water droplets suspended in a dry air stream. So far, there is no correlation that is strictly applicable for the high-pressure flow boiling conditions that we are interested in for the PWR DNB application. Nonetheless, given the physical basis as well as the ease of implementation in the CFD code, we can think of a better option among the models available in the literature. In this study, the Kim-Park condensation model,[25] which was developed for condensing bubbles in a subcooled water pool, was implemented into the associated closure model instead of the Ranz-Marshall model. The Kim-Park correlation for the condensate Nusselt number Nu_c is given by

$$Nu_c = 0.2575 Re_b^{0.7000} Ja_l^{-0.2043} Pr_l^{-0.4564} \quad , \qquad (20)$$

where

Re_b = bubble Reynolds number, $\frac{\rho_l U_{rel} D_b}{\mu_l}$

Ja_l = Jacob number of subcooled liquid, $\frac{\rho_l C_{p,l}(T_{sat}-T_l)}{\rho_g h_{fg}}$

Pr_l = Prandtl number of subcooled liquid, $\frac{C_{p,l}\mu_l}{k_l}$.

Note that Eq. (20) estimates Nu_c as infinite when the liquid temperature approaches the saturation point (i.e., Ja_l in the denominator approaches 0 as $T_l \rightarrow T_{sat}$). To avoid any numerical issues that may arise from Eq. (20), Ja_l is defined as follows:

$$Ja_l = \frac{\rho_l C_{p,l}(T_{sat} - \min(T_{sat} - 10^{-7}, T_l))}{\rho_g h_{fg}} \quad . \qquad (21)$$

A comparison is made for two high-pressure (i.e., 147 bars) tests, T34 and T37, with both the Ranz-Marshall correlation versus the Kim-Park correlation.[26] It is observed from both test cases that the point of net vapor generation is predicted earlier when the Kim-Park correlation is employed. This observation is consistent for the other simulation case: T1 performed at P = 45 bars. In general, when used in conjunction with the S-gamma model, the Kim-Park correlation tends to better predict the point of net vapor generation measured from the experiments. Given the physical suitability over the Ranz-Marshall correlation as well as the predictive performance observed, the Kim-Park correlation is preferred for the present high-pressure boiling simulations. It is noted, however, that the Kim-Park correlation is originally developed only for predicting the Nusselt number Nu_c during condensation, and Eq. (21) forces a small value of the subcooled liquid Jacob number when the bulk liquid is superheated ($T_l > T_{sat}$). Therefore, the present approach has an inherent limitation in accurately predicting the effect of bulk boiling in the superheated liquid near the heater surface. Note that the current boiling closure selection is largely targeted for subcooled flow boiling and associated DNB prediction performance, so admittedly, the effect of bulk boiling on DNB is not fully investigated in the interfacial heat transfer model tests.

IV.D. Overall Predictive Performance over Experimental Measurements

Based on the results from closure sensitivity study in Secs. IV.A~IV.C, a new model setup was proposed for the FY19 CASL boiling model. A comparison was made to assess the capability of the proposed boiling model, compared to the FY17 model (see Table III), at particularly high-pressure PWR-like operating conditions. Figure 7 reports the void profile prediction by the FY17 model (Fig. 7a) and the proposed FY19 model (Fig. 7b) against the Bartolomei data measurement at pressures of about 150 bars. It clearly shows that the FY17 model consistently overestimates the experimental data with significantly earlier prediction of the net vapor generation along the heated length, whereas the proposed model shows much better agreement with the Bartolomei data for all five test cases applying the different heat fluxes. The comparison presented in Figs. 7c and 7d also shows similar improvement by the proposed model. It is noted that these comparative studies as well as the sensitivity study discussed in Secs. IV.A through IV.C were considered to determine the Gen1-FY19 CASL boiling closure selection shown in Table I. While notable improvement is observed with the proposed boiling model shown below, the comparisons against the experimental data are based only on the spatially averaged void measurements, and interfacial momentum closures such as lift and wall lubrication force are not tested. Thus, it is still limited to prove the validity of the proposed boiling model for high-fidelity lateral void distribution in subcooled boiling applications. This also implies a potential research area for DNB closure sensitivity study with regard to both axial and lateral void profiles when associated experimental data are available at high-pressure conditions.

V. RESULTS OF DNB PREDICTIVE PERFORMANCE, VOID DISTRIBUTION

We performed a virtual boiling test with the GEN-1 model to create a total boiling curve history up to the DNB point, which exactly follows experimental boiling test protocols. A detailed description of the virtual boiling test in the M-CFD framework is reported in the authors' previous publications. An example of a DNB detected virtual boiling test for pipe flow configuration is illustrated in Fig. 8.

As shown above, the DNB occurance is determined by monitoring the wall superheated temperature in the incrementally applied heat flux scenario. In the current test, the heat flux is increased by 0.05 MW/m^2 to emulate the thermal equilibrium condition at each stage. While the outlet temperature and net void value are monitored to check the energy balance, the key DNB detection is mainly determined by the temperature excursion in which the heat transfer mode is transitioning from the nucleate boiling regime into a vapor heat transfer regime. As highlighted in the blue circle in Fig. 8, the wall temperature is clearly spiking when the heat flux is getting close to the CHF condition. Moreover, the trend of the wall temperature represents the three modes of heat transfer over the incremental heat flux condition: single-phase heat transfer (low heat flux), nucleate boiling heat transfer (intermdeaite heat flux) and DNB (close to the CHF). The temperature excursion takes place near the heat flux of 1.9 MW/m^2. For an applied heat flux greater than 1.9 MW/m^2, the regime is beyond the DNB condition. Beyond DNB, the wall temperature does not converge and becomes unstable even though the simulation runs for sufficient iterations.

In previous validation tests with the FY17 CASL boiling model, we found that the model exhibits consistent trends of underprediction of DNB in the simulation

TABLE III

Selected Closure Comparison Between Gen1-FY17 and Gen1-FY19

Selected Closures	GEN1-FY17 (Original)	GEN1-FY19 (Modified)
Lift force	No Lift	Sugrue lift[13]
Wall lubrication force	No wall lubrication modeled	Lubchenko et al. model[14]
Condensation model	Ranz-Marshall[24]	Kim-Park[25]
Interfacial area density	Spherical particle assumption	Symmetric assumption
Interfacial length scale	Kurul-Podowski model[15]	S-gamma model[27]
Bubble departure diameter	Tolubinsky and Kostanchuk[28]	Kocamustafaogullari[18]
Bubble departure frequency	Cole[19]	Cole[19]
Nucleation site density	Lemmert-Chawla[22]	Modified Li et al. model[17]

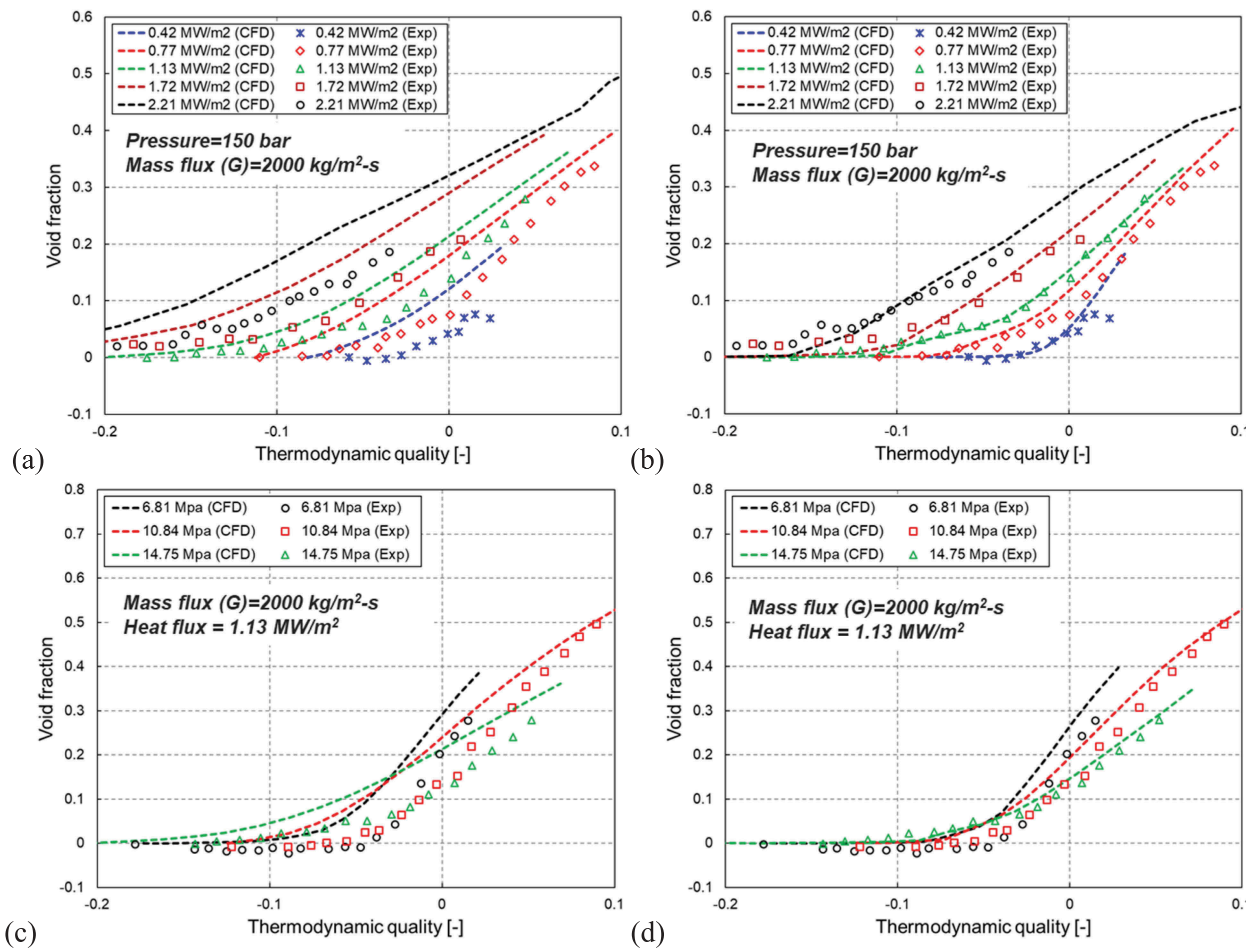

Fig. 7. Comparison of CFD predictions by (a) and (c) the FY17 model and (b) and (d) the FY19 model against Bartolomei experimental data with a range of pressure and heat flux conditions.

compared to the measurements. Overall deviations between measurement and calculation turn out to be around 33% in the pipe flow test and 30% to 50% underpredicted behavior in the 5 × 5 fuel bundle tests. Interestingly, notable underpredicted model behaviors are observed with the mixing vane featured fuel bundle channel. It is believed that the turbulence mixing effect is more pronounced in the mixing vane flow channel and results in a larger deviation compared to the experiments. One of the potential causes for underprediction of DNB would be possible overprediction of void creation at the heated wall due to inappropriate wall boiling closure, which might not be applicable for the high-pressure condition. As discussed in Sec. IV, void creation in a subcooled boiling simulation is largely determined by an evaporation heat flux term on the wall and some extent of the lateral distribution term by interfacial momentum. Evaporation heat flux determines void mass flux at the heated wall as a void source term. Therefore, nonrepresentative wall boiling closure for high pressure could lead to overprediction of void creation, and the overpredicted void will trigger DNB detection at the low heat flux condition. Thus, underpredicted DNB values are readily obtained in most of the tests so far. Another issue would be incorrect void distribution due to inappropriate interfacial momentum transfer closure. Among many interfacial closures, lift force and wall lubrication force would be the most relevant components that determine a lateral void fraction near the wall.

Admittedly, the conjugate heat transfer between the solid and the fluid is not modeled in the current study. The heat flux is directly applied to the fluid surface where thermal contact is made at the pipe surface. The effect of the conjugate heat transfer on the surface temperature prediction might be nontrivaial when the flow channel is more complex, such as fuel buddle application in the PWR design. As the focus on the current study is to finalize the optimal and robust closure selection for

 ANS

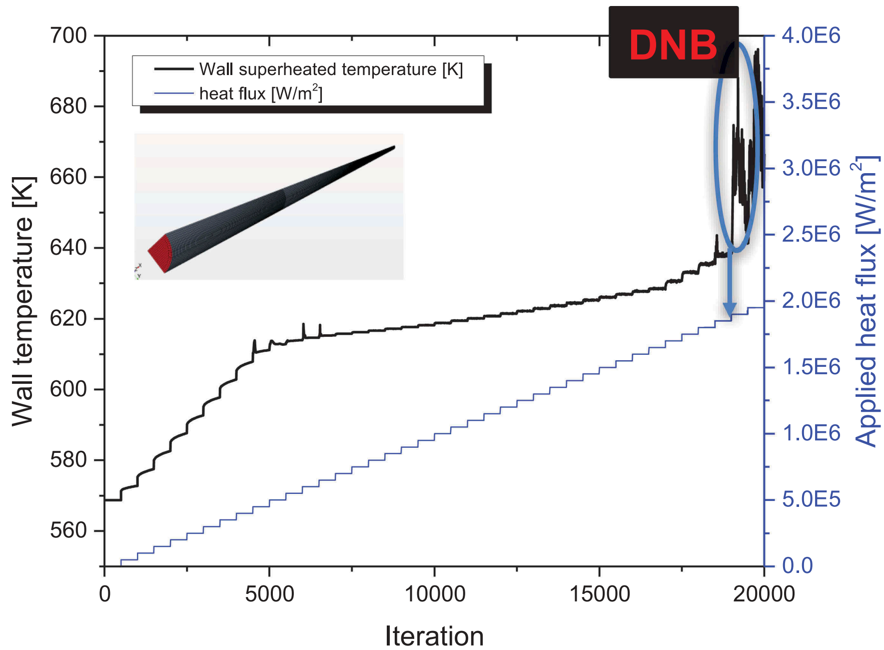

Fig. 8. Maximum wall temperature behavior with incremented heat flux up to DNB point in which notable temperature excursion is observed.

two-phase DNB application, the thermal interaction between solid and fluid is not considered a high priority.

V.A. DNB Performance Comparison Between Original Model and Modified Model

In this paper, we report the comparative study of the DNB performance with the modified Gen1-FY19 model against the original boiling model used in the previous campaign. While the Gen1-FY19 model is feasible to apply the complex flow channel like the 5 × 5 fuel bundle case, we largely focused on the pipe flow DNB validation in order to evaluate the sensitivity of the newly selected closure model for high-pressure DNB applications. The virtual boiling test and DNB detection mechanism are identical to the method tested in the previous validation tests. For example, an operation test condition is selected from the DNB experimental report, a representative mesh is built up, and a controlled heat flux profile (e.g., an incremental heat flux for the heated surface in the computational domain) is set for the virtual boiling test up to the DNB occurrence. The only change is a combination of selected closures in wall boiling and interfacial transfer terms. To clearly compare the difference in the selected closure setting, a comparison table is summarized in Table III. The closures not mentioned below are set to be identical to Table I.

The overall predictive performance of the DNB simulation is improved with a modified boiling model as summarized in Fig. 9. Those improvements in DNB performance should be further investigated in terms of robustness and applicability in the various flow channel designs such as fuel bundle configurations with and without mixing vane spacers. From the numerical robustness standpoint, most tests in the current study (e.g., pipe flow configuration) demonstrate a viable numerical robustness and stability up to the DNB point. However, it is worth noting that some of the high subcooled test conditions still exhibit some numerical instability when the heat flux is close to the DNB point. This numerical instability issue should be further investigated in both closure sensitivity level tests and DNB tests in a complex flow channel test. In parallel to the pipe flow DNB study, the Westinghouse proprietary design of the 5 × 5 fuel bundle DNB simulation was conducted with the modified boiling model, and the associated results of the 5 × 5 fuel bundle test can be referenced in Brewster et al.'s work.[29]

Among the current test results, the DNB performance is reviewed along with different subcooled temperatures. Five test cases with different subcooled conditions are carefully selected while all other operating conditions are kept identical. The subcooled temperature varies from 12 to 60 K, and two different subcooled groups are divided as follows: one group with low subcooled condition (less than 35 K subcooled from the saturation temperature) and the other group with high subcooled condition (more than 40 K subcooled inlet temperature). Interestingly the low subcooled group shows notably good predictive capabilities (exhibiting less

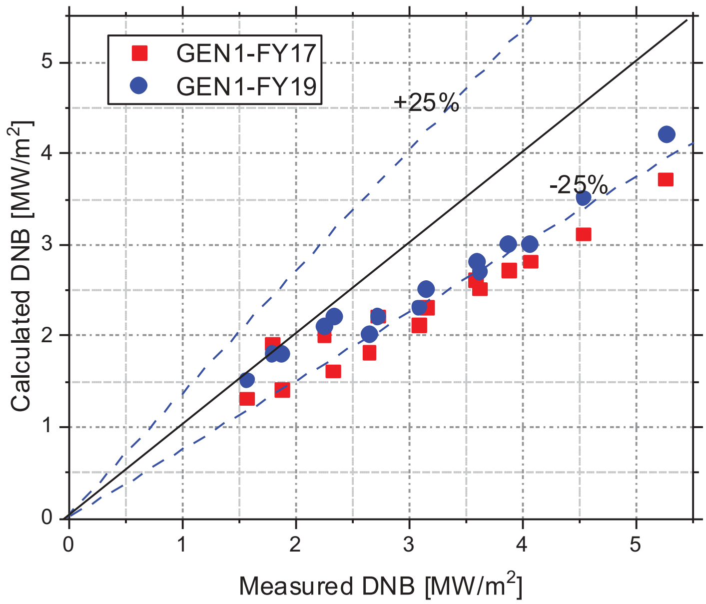

Fig. 9. Prediction performance evaluation for GEN1-FY17 and GEN1-FY19.

than 7% deviation from the measurements) while the high subcooled group makes a relatively larger deviation compared to the low subcooled group. This observation indicates that the modified boiling model is well calibrated to the low subcooled flow boiling application and quenching closure needs to be further investigated for the high subcooled flow boiling application. It is believed that the bubble influence area coefficient and bubble growth waiting time in Eq. (13) should be readjusted for high subcooled flow boiling application at high-pressure conditions. Those kinds of closure adjustments require appropriate experimental measurements from a high-resolution flow visualization technique.

V.B. Radial Void Profile Characteristics with Elevating Heat Flux Conditions

Here, we report the temperature and corresponding density and void distribution calculated from the DNB simulation. At any given heat flux condition, the two-fluid approach will solve all of the fluid parameters in both phases as well as three-dimensional void distribution. Figure 10 graphically illustrates those calculated fluid parameters and potential DNB locations in the pile flow application.

Generally, DNB occurs at the end of the heated section when the heat flux is uniformly applied. So, a monitoring line probe is used to extract the radial void profile at the end of the heated location; here, $z = 500$ mm from the inlet of the pipe. A radial void distribution is reported along with four different heat flux conditions (24%, 50%, 75%, and 82.5% of CHF) as illustrated in Fig. 11. The horizontal axis is the radial position starting from the centerline of the bulk flow region (0.0 mm) to the near-wall region (3.85 mm). The vertical axis represents the corresponding void fraction. As the heat flux increases, the wall boiling model kicks in and introduces wall boiling by producing bubbles from the wall. The void fraction near the wall is accumulated above 0.6 when the heat flux becomes 50% of CHF. The void profile observed in the current study indicates a wall-peak trend, which is observed in most subcooled flow boiling experiments with low void quality condition. Near-wall voids tend beyond 0.9 when the heat flux gets close to 82.5% of CHF.

Without modifying the DNB triggering criterion (e.g., Y+ of 200 and local void of 0.9), the underpredicted DNB in the current approach might be further improved by recalibrating the wall boiling closure for the high-pressure application as well as interfacial momentum transfer. Unfortunately, most of the DNB test does not record any of the wall boiling dynamics (bubble departure size, shape, nucleation size, departure frequency, waiting time, etc.) but focuses only on the DNB measurement. Thus, the lack of those bubble dynamic measurement or experimental boiling curve data significantly hinders the current DNB validation tests. In addition to the wall boiling validation, there must be huge room to improve the interfacial momentum closures (e.g., lift force, wall lubrication force, and mean bubble diameter) in the modeling if associated experimental data from either the adiabatic two-phase test or the boiling test at a high-pressure condition are available. This experimental research support should be more addressed in the future tasks of the CFD-based DNB simulation application.

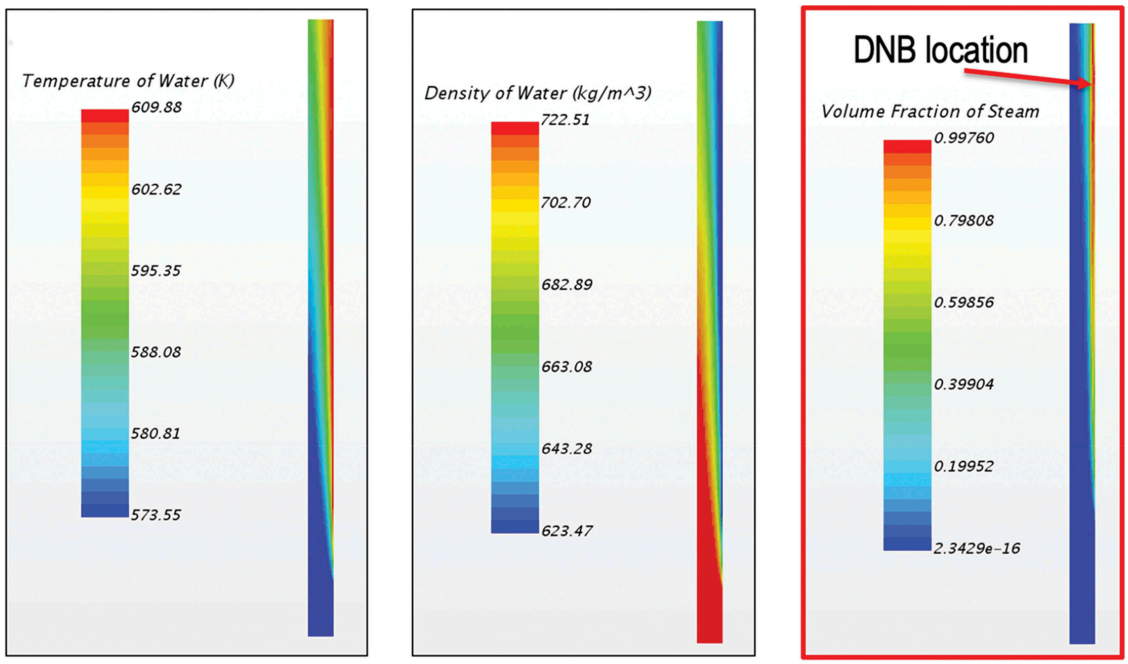

Fig. 10. An example of axial and radial profiles of temperature, density, and void for the DNB test (uniform heat flux applied on the right side of each figure).

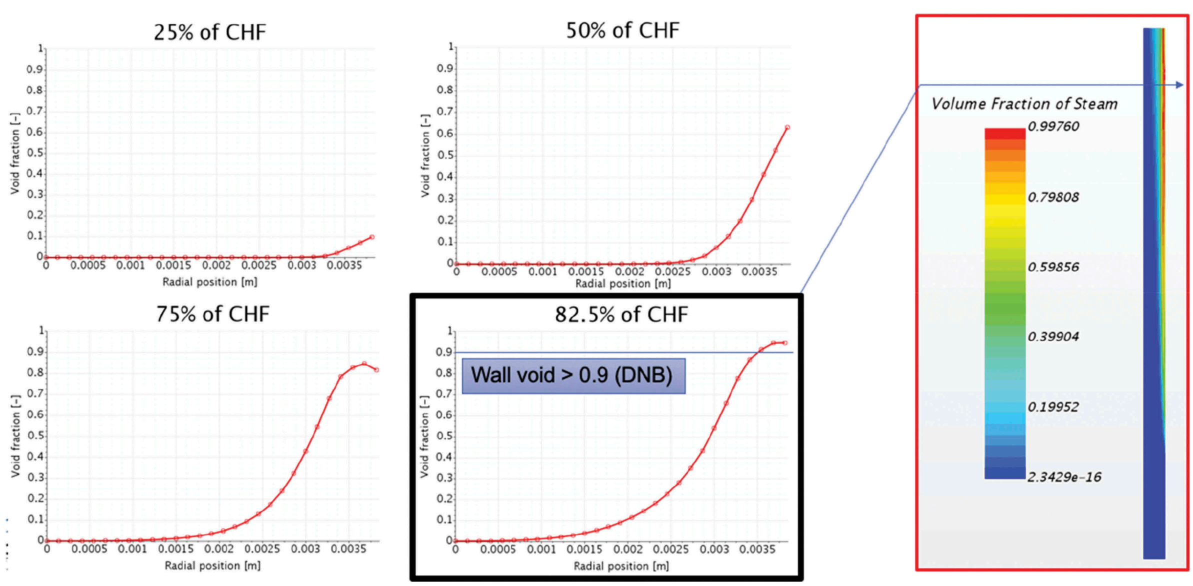

Fig. 11. Radial void distribution along with increasing heat flux up to 82.5% of CHF.

VI. CONCLUSIONS AND SUGGESTED FUTURE WORK

Over the past 4 years, the CASL THM team has extensively investigated a state-of-the-art M-CFD approach to provide a high-fidelity DNB simulation capability based on the two-fluid Eulerian framework in conjunction with a wall heat flux partitioning model. The overarching goal in this task is to develop and demonstrate a robust M-CFD model capable of predicting the DNB value for high-pressure subcooled flow boiling for PWR application. A robust and physically well represented boiling closure model is proposed based on a series of previous studies. The Gen1-FY19 DNB model is evaluated with reference to experimental measurement resulting in an improved predictive trend compared to the original model. A high-level summary of the current study and some suggested future work are the following:

1. The CASL baseline model was developed, and DNB prediction methodology using the M-CFD approach was proposed to evaluate the predictive performance.

2. Predicated DNB values with the original CASL model (i.e., Gen1-FY17) were compared against the measurements in various flow configurations indicating underpredictive behavior up to 33% (pipe flow case) and 50% (fuel bundle with and without mixing vane cases). Note that the mixing vane test case exhibits a relatively larger deviation compared to the without mixing vane test.

3. We scrutinized the baseline boiling model and identified what would be the potential cause of underprediction. Based on a closure sensitivity study, a modified boiling closure model (i.e., Gen1-FY19) is introduced with the following changes:

   a. Improved wall boiling closure for high-pressure subcooled boiling applications. Newly calibrated BDD and NSD are implemented.

   b. Realistic interfacial momentum transfer closures (a bubble shape considereing lift and wall lubrication forces and advanced bubble size distribution with the S-gamma model) are applied.

   c. The bulk region condensation model is modified.

4. The modified boiling model exhibits an improved DNB predictive behavior against the original model while maintaining a viable robustness in the virtual boiling test.

5. If experimental measurements for high-pressure subcooled boiling are available, the modified boiling model should be further validated with more than just DNB values such as axial and radial void profiles along with flow channel, wall superheated condition, and wall boiling characteristics.

6. Nonetheless, the Gen1-FY19 model is still a feasible option for high-pressure DNB application with reasonable accuracy (less than 24% deviation from the measurements) while viable robustness is achieved in most of the tests. In addition, at PWR-like subcooled conditions (subcooling level below 40 K and high pressure), the current model demonstrates an even improved predictive trend (the deviation falls below 7%).

Acknowledgments

The authors greatly acknowledge all of the THM team members from Idaho National Laboratory, Massachusetts Institute of Technology, Los Alamos National Laboratory (LANL), Westinghouse Electric Company, and Oak Ridge National Laboratory who have contributed in finalizing CASL boiling model framework through many meeting and technical consultations over the past years. Also, deep appreciation is extended to the Civilian Nuclear Program Office and LANL Institutional Computing for steady support on the program.

ORCID

Seung Jun Kim http://orcid.org/0000-0002-6913-6358

References

1. S. J. KIM, L. ZOU, and B. JONES, "An Experimental Study on Subcooled Flow Boiling CHF of R134a at Low Pressure Condition with Atmospheric Pressure (AP) Plasma Assisted Surface Modification," *Int. J. Heat Mass Transfer*, **81**, 362 (2015); https://doi.org/10.1016/j.ijheatmasstransfer.2014.10.032.
2. S. J. KIM, E. BAGLIETTO, and E. DEMARLY, "Evaluation of DNB Predictive Capability in Multiphase Boiling Model of STAR-CCM+," LA-UR-16-28815, Los Alamos National Laboratory (2016).
3. S. J. KIM, "Evaluation of CASL Boiling Model for DNB Performance in Full Scale 5 × 5 Fuel Bundle with Spacer Grids," LA-UR-17-21026, Los Alamos National Laboratory (2017).
4. S. J. KIM, "A Status Review on DNB Prediction Using CASL Baseline Boiling Model and Possible Suggestions Regarding Wall Boiling Closures," LA-UR-18-28198, Los Alamos National Laboratory (2018).
5. S. J. KIM, "Assessments on DNB Performance for High Pressure Subcooled Boiling with Modified CASL Boiling Model," LA-UR-19-28666, Los Alamos National Laboratory (2019).
6. J. YOO and E. BAGLIETTO, "A Parametric CFD Boiling Study Using State of Art Two-Phase and Boiling Closure Models," *Proc. 18th Int. Topl. Mtg. Nuclear Reactor Thermal Hydraulics (NURETH-18)*, Portland, Oregon, August 18–22, 2019, American Nuclear Society (2019).
7. J. WEISMAN and B. PEI, "Prediction of Critical Heat Flux in Flow Boiling at Low Qualities," *Int. J. Heat Mass Transfer*, **26**, *10*, 1463 (1983); https://doi.org/10.1016/S0017-9310(83)80047-7.
8. J. R. COOPER, "IAPWS Industrial Formulation 1997 for the Thermodynamic Properties of Water and Steam," The

ANS

International Association for the Properties of Water and Steam (2007).

9. B. MAGOLAN and E. BAGLIETTO, "Assembling a Bubble-Induced Turbulence Model Incorporating Physical Understanding from DNB," *Int. J. Multiphase Flow*, **116**, 185 (2019); https://doi.org/10.1016/j.ijmultiphaseflow.2019.04.009.

10. R. J. WEATHERHEAD, "Nucleate Boiling Characteristics and the Critical Heat Flux Occurrence in Subcooled Axial-Flow Water Systems," ANL-6675, Argonne National Laboratory.

11. S. KIM et al., "CFD Study of a Multi-Phase Subcooled Flow Boiling Model and the Evaluation of the Model's Predictive Capability for Boiling Characterisitcs," *Proc. 11th Int. Topl. Mtg. Nuclear Reactor Thermal-Hydraulics, Operation and Safety (NUTHOS-11)*, Gyeongju, Korea, October 9–13, 2016.

12. A. TOMIYAMA et al., "Drag Coefficients of Single Bubbles Under Normal and Micro Gravity Conditions," *JSME Int. J. Ser. B*, **41**, 472 (1998); https://doi.org/10.1299/jsmeb.41.472.

13. R. SUGRUE, "A Robust Momentum Closure Approach for Multiphase Computational Fluid Dynamics Applications," Doctoral Dissertation, Massachusetts Institute of Technology (2017).

14. N. LUBCHENKO et al., "A More Fundamental Wall Lubrication Force from Turbulent Dispersion Regularization for Multiphase CFD Applications," *Int. J. Multiphase Flow*, **98**, 36 (2018); https://doi.org/10.1016/j.ijmultiphaseflow.2017.09.003.

15. N. KURUL and M. PODOWSKI, "On the Modeling of Multidimensional Effects in Boiling Channels," *Proc. 27th Natl. Heat Transfer Conf.*, Minneapolis, Minnesota, July 28–31, 1991, American Nuclear Society (1991).

16. S. LO and P. RAO, "Modeling of Droplet Breakup and Coalescence in an Oil-Water Pipeline," *Proc. 6th Int. Conf. Multiphase Flow (ICMF2007*), Leipzig, Germany, 2007.

17. Q. LI et al., "Development, Verification and Application of a New Model for Active Nucleation Site Density in Boiling System," *Nucl. Eng. Des.*, **328**, 1 (2018); https://doi.org/10.1016/j.nucengdes.2017.12.027.

18. G. KOCAMUSTAFAOGULLARI, "Pressure Dependence of Bubble Departure Diameter for Water," *Int. Commun. Heat Mass Transfer*, **10**, *6*, 501 (1983); https://doi.org/10.1016/0735-1933(83)90057-X.

19. R. COLE, "A Photographic Study of Pool Boiling in the Region of the Critical Heat Flux," *AIChE J.*, **6**, *4*, 544 (1960); https://doi.org/10.1002/()1547-5905.

20. G. BARTOLOMEI and V. CHANTURIYA, "Experimental Study of True Void Fraction When Boiling Subcooled Water in Vertical Tubes," *Therm. Eng.*, **14**, *2*, 123 (1967).

21. G. BARTOLOMEI et al., "An Experimental Investigation of True Volumetric Vapor Content with Subcooled Boiling in Tubes," *Therm. Eng.*, **29**, *3*, 132 (1982).

22. M. LEMMERT and J. CHAWLA, "Influence of Flow Velocity on Surface Boiling Heat Transfer Coefficient," *Heat Transf. Boiling*, **237**, 247 (1977).

23. T. HIBIKI and M. ISHII, "Active Nucleation Site Density in Boiling Systems," *Int. J. Heat Mass Transfer*, **46**, *14*, 2587 (2003); https://doi.org/10.1016/S0017-9310(03)00031-0.

24. W. RANZ and W. MARSHALL, "Evaporation from Drop," *Chem. Eng. Prog.*, **48**, *3*, 141 (1952).

25. S.-J. KIM and G.-C. PARK, "Interfacial Heat Transfer of Condensing Bubble in Subcooled Boiling Flow at Low Pressure," *Int. J. Heat Mass Transfer*, **54**, *13*, 2962 (2011); https://doi.org/10.1016/j.ijheatmasstransfer.2011.03.001.

26. J. YOO and E. BAGLIETTO, "CFD Boiling Validation: Closure Model Assessment and Discussion on the Improvement of CASL Boiling Model for High-Pressure Subcooled Boiling Flow," INL/EXT-19-55963, Idaho National Laboratory (2019).

27. "SIEMENS START-CCM+ Version 12.06 Tutorial" (2018); https://steve.cd-adapco.com/.

28. V. TOLUBINSKY and D. KOSTANCHUK, "Vapour Bubbles Growth Rate and Heat Transfer Intensity at Subcooled Water Boiling," *Proc. Int. Heat Transfer Conf. 4*, Paris-Versailles, France, August 31–September 5, 1970.

29. R. BREWSTER, J. FENG, and E. BAGLIETTO, "Industry Application of CASL DNB Methods," L2.THM.DNB.P19.01, Consortium for Advanced Simulation of Light Water Reactors (2019).